

Constraints from joint analysis of CMB, and tSZ cluster counts and power spectrum

Laura Salvati¹, Marian Douspis¹, and Nabila Aghanim¹

Institut d'Astrophysique Spatiale, CNRS (UMR 8617) Université Paris-Sud, Bâtiment 121, Orsay, France e-mail: laura.salvati@ias.u-psud.fr

ABSTRACT

Thermal Sunyaev-Zel'dovich effect is one of the recent probes of cosmology and large scale structures. We update constraints on cosmological parameters from galaxy clusters observed by the Planck satellite in a first attempt to combine cluster number counts and power spectrum of hot gas, using the new value of the optical depth, and sampling at the same time on cosmological and scaling-relation parameters. We find that in the Λ CDM model, the addition of tSZ power spectrum provides only small improvements with respect to number counts only, leading to the 68% c.l. constraints $\Omega_m = 0.32 \pm 0.02$, $\sigma_8 = 0.77 \pm 0.03$ and $\sigma_8(\Omega_m/0.3)^{1/3} = 0.78 \pm 0.03$ and lowering the discrepancy with CMB primary anisotropies results (updated with the new value of τ) to $\simeq 1.6\sigma$ on σ_8 . We analyse extensions to standard model, considering the effect of massive neutrinos and varying the equation of state parameter for dark energy. In the first case, we find that the addition of tSZ power spectrum helps in strongly improving cosmological constraints with respect to number counts only results, leading to the 95% upper limit $\sum m_\nu < 1.53$ eV. For the varying dark energy EoS scenario, we find again no important improvements when adding tSZ power spectrum, but still the combination of tSZ probes is able in providing constraints, producing $w = -1.0 \pm 0.2$. In all cosmological scenari the mass bias to reconcile CMB and tSZ probes remains low: $(1-b) \lesssim 0.66$ as compared to estimates from weak lensing and Xray mass estimate comparisons or numerical simulations.

Key words. Cosmology – SZ effect – galaxy clusters

1. Introduction

Galaxy clusters are the most massive bound structures emerging in the cosmic web of large-scale structure (LSS). These objects are associated with peaks in the matter density field on megaparsec scales, whose abundance is strongly sensitive to both growth of structure and matter density. Thus, the abundance of these peaks is strongly dependent on the underlying cosmological model and it provides constraints on cosmological parameters, see e.g. Allen et al. (2011).

These constraints are even more powerful when combined with, or compared to, results from other observables, in particular primary temperature and polarization anisotropies of Cosmic Microwave Background (CMB) radiation and Baryon Acoustic Oscillations (BAO). On the one hand, comparing results from different observables provides important consistency checks. On the other hand, the combination of geometrical and growth-based probes can improve constraints on parameters such that the equation of state (EoS) for dark energy, because of the different degeneracies between parameters for the different probes.

The key feature of galaxy clusters consists in their multi-component nature, which allows them to provide information at different wavelengths, see again Allen et al. (2011). During last years, several measurements of cluster samples in the X-rays (Boehringer et al. 2017; Chon & Boehringer 2012), optical (Rykoff et al. 2016) and millimetre (mm) (Bleem et al. 2015, South Pole Telescope, SPT), (Marriage et al. 2011, Atacama Cosmology Telescope, ACT), (Planck

Collaboration 2014d, 2016f, Planck) wavelengths have improved the constraints on cosmological parameters.

In this work, we focus on galaxy clusters observed in the mm wavelengths through thermal Sunyaev-Zel'dovich (tSZ) effect (Sunyaev & Zeldovich 1970), i.e. the inverse Compton scattering between CMB photons and hot electrons in the intra-cluster medium (ICM), using measurements of the Planck satellite (Planck Collaboration 2016a,f). In particular, we exploit the combination of galaxy cluster number counts and angular power spectrum of warm-hot gas seen in SZ by Planck (Planck Collaboration 2016d) and SPT (George et al. 2015). We try to quantify if and how the addition of current tSZ power spectrum data helps in better breaking the degeneracy between the cosmological parameters and the ones used to model the physics of the clusters.

In light of the discrepancy between CMB and number counts constraints (Planck Collaboration 2014b), we compare our results with most recent CMB data from Planck Collaboration (2016b,g) for Λ CDM model. We also explore results obtained relaxing some assumptions of the standard model, in particular considering the sum of the neutrino masses, $\sum m_\nu$, and the dark energy EoS parameter, w , as varying parameters. We show how our combined analysis improves constraints on these extensions of the standard model.

This paper is organized as follows: in section 2 we briefly describe the theoretical model needed to build the number counts for galaxy clusters, observed through tSZ effect, and the tSZ power spectrum. In section 3 we describe the approach we use in this analysis and in section 4 we show our

results. In sections 5 and 6 we derive our final discussion and conclusions.

2. tSZ cosmological probes

Thermal Sunyaev-Zel'dovich effect is a powerful cosmological probe. Its main property is the fact that surface brightness of tSZ effect is redshift-independent, therefore providing nearly mass-limited cluster samples from high-resolution mm surveys, at arbitrarily high redshift. The ability to sample up to high redshifts ensures us to track with high accuracy the evolution of large scale structure in particular unabling us to constrain neutrino mass, thanks to their effect on large scale structure evolution, i.e. the damping of matter power spectrum at small scales, see e.g. [Lesgourgues & Pastor \(2012\)](#).

The intensity of tSZ effect, in a given direction of the sky $\hat{\mathbf{n}}$, is measured through the thermal Compton parameter y , defined as

$$y(\hat{\mathbf{n}}) = \int n_e \frac{k_B T_e}{m_e c^2} \sigma_T ds, \quad (1)$$

where k_B is the Boltzmann constant, σ_T is the Thomson scattering cross section and m_e , n_e and T_e are respectively the electron mass, number density and temperature.

In defining clusters detected through tSZ effect, we adopt the following convention: we define the cluster mass M_{500} as the total mass contained in a sphere of radius R_{500} , defined as the radius within which the cluster mean mass overdensity is 500 times the critical density at that redshift, i.e.

$$M_{500} = \frac{4\pi}{3} R_{500}^3 500 \rho_c(z), \quad (2)$$

where the critical density is defined as

$$\rho_c(z) = \frac{3H^2(z)}{8\pi G} \quad (3)$$

with $H(z)$ being the Hubble parameter.

We consider therefore the following observables for clusters detection from [Planck Collaboration \(2016f\)](#): Y_{500} , which is the the Compton y -profile integrated within a sphere of radius R_{500} , and the cluster angular size θ_{500} .

2.1. Number counts

The predicted number of clusters observed by a given survey in a redshift bin $[z_i, z_{i+1}]$ is given by

$$n_i = \int_{z_i}^{z_{i+1}} dz \frac{dN}{dz}, \quad (4)$$

where

$$\frac{dN}{dz} = \int d\Omega \int_{M_{\min}}^{M_{\max}} dM_{500} \hat{\chi}(z, M_{500}; l, b) \frac{dN}{dz dM_{500} d\Omega}, \quad (5)$$

where $\hat{\chi}(z, M_{500}; l, b)$ is the survey completeness at a given position in the sky (l, b) and

$$\frac{dN}{dz dM_{500} d\Omega} = \frac{dN(M_{500}, z)}{dM_{500}} \frac{dV_c}{dz d\Omega} \quad (6)$$

is the product between the comoving volume element (per unit redshift and solid angle) $dV_c/dz d\Omega$ and the mass function $dN(M_{500}, z)/dM_{500}$. The latter represents the probability of having a galaxy cluster of mass M at redshift z , in the direction given by $d\Omega$.

This description can be generalized for number counts being function also of the signal-to-noise ratio, see ([Planck Collaboration 2016e](#)).

2.2. tSZ power spectrum

The complete analytical description of tSZ power spectrum has been fully covered in different papers, such as [Komatsu & Seljak \(2002\)](#) and [Planck Collaboration \(2014c\)](#), therefore we report here only the necessary results.

Considering the halo-model (see e.g. [Cooray \(2000\)](#)), we can write tSZ power spectrum as the sum of one-halo and two-halo terms

$$C_\ell^{\text{tSZ}} = C_\ell^{\text{1 halo}} + C_\ell^{\text{2 halo}}. \quad (7)$$

In the flat sky limit ($\ell \gg 1$), the one-halo term is expressed as

$$\begin{aligned} C_\ell^{\text{1 halo}} &= \int_0^{z_{\max}} dz \frac{dV_c}{dz d\Omega} \\ &\times \int_{M_{\min}}^{M_{\max}} dM \frac{dN(M_{500}, z)}{dM_{500}} |\tilde{y}_\ell(M_{500}, z)|^2 \\ &\times \exp\left(\frac{1}{2} \sigma_{\ln Y^*}^2\right). \end{aligned} \quad (8)$$

The term $\tilde{y}_\ell(M_{500}, z)$ is the Fourier transform on the sphere of the Compton parameter y of individual clusters and is given by (using Limber approximation):

$$\begin{aligned} \tilde{y}_\ell(M_{500}, z) &= \frac{4\pi r_s}{\ell_s^2} \left(\frac{\sigma_T}{m_e c^2} \right) \\ &\times \int_0^\infty dx x^2 P_e(M_{500}, z, x) \frac{\sin(\ell_x/\ell_s)}{\ell_x/\ell_s}, \end{aligned} \quad (9)$$

where r_s is the scale radius of the 3D pressure profile $P_e(M_{500}, z, x)$, $\ell_s = D_A(z)/r_s$ (with $D_A(z)$ being the angular diameter distance) and $x = r/r_s$. We use the universal pressure profile provided by [Arnaud et al. \(2010\)](#). The term $\sigma_{\ln Y^*}$ represents the dispersion in the scaling relations that will be fully described in the next section.

The two-halo term ([Komatsu & Kitayama 1999](#)) is derived from computing the correlation between two different halos as

$$\begin{aligned} C_\ell^{\text{2 halo}} &= \int_0^{z_{\max}} dz \frac{dV_c}{dz d\Omega} \\ &\times \left[\int_{M_{\min}}^{M_{\max}} dM \frac{dN(M_{500}, z)}{dM_{500}} \tilde{y}_\ell(M_{500}, z) B(M_{500}, z) \right]^2 \\ &\times P(k, z), \end{aligned} \quad (10)$$

where $P(k, z)$ is the matter power spectrum and $B(M, z)$ is the time-dependent linear bias factor. This last term relates the matter power spectrum to the power spectrum of the cluster correlation function. We follow [Komatsu & Kitayama \(1999\)](#) and use the definition

$$B(M_{500}, z) = 1 + \frac{\nu^2(M_{500}, z)}{\delta_c(z)}, \quad (11)$$

where $\nu(M_{500}, z) = \delta_c(M_{500})/D(z)\sigma(M_{500})$, with $\sigma(M_{500})$ being the present-day rms mass fluctuation, $D(z)$ the linear growth factor and $\delta_c(z)$ the threshold over-density of spherical collapse.

Following the analysis of Komatsu & Seljak (2002) and Horowitz & Seljak (2017), in order to have an accurate error evaluation, we take into account also the contribution from the trispectrum term, $T_{\ell\ell'}$, which is the harmonic-space four-point function and represents the non-gaussian contribution of the cosmic variance. The dominant term in the halo model is defined as (Cooray 2001; Komatsu & Seljak 2002):

$$\begin{aligned} T_{\ell\ell'} &\simeq \int_0^{z_{\max}} dz \frac{dV_c}{dz d\Omega} \\ &\times \int_{M_{\min}}^{M_{\max}} dM \left[\frac{dN(M_{500}, z)}{dM_{500}} \right. \\ &\times \left. |\tilde{y}_\ell(M_{500}, z)|^2 |\tilde{y}_{\ell'}(M_{500}, z)|^2 \right]. \end{aligned} \quad (12)$$

2.3. Assumptions on the modelling ingredients

There are some major uncertainties in constraining cosmological parameters from galaxy clusters, related to the ingredients needed to build the theoretical model described in previous section. In fact the theoretical mass function needs to be transformed into a prediction for the distribution of clusters, in the space of survey observables. The first uncertainty is therefore related to an imperfect knowledge of the scaling relations between the cluster mass and the survey observable, that is used as a proxy for this quantity. The second one is related to the model of the selection process, which needs to be accurately built, in order to avoid possible selection biases that could affect final results on cosmological parameters constraints.

Thus, in order to completely determine the theoretical model, we need some assumptions on scaling relations, mass function and selection function. Regarding the latter, it is out of the scope of this paper, we therefore refer to the complete discussion reported in Planck Collaboration (2016e).

2.3.1. Scaling Relations

A crucial element in modelling the cosmological probes is the exact evaluation of clusters mass and therefore of the scaling relations between survey observables and mass. For all details on the evaluation of these relations for Planck observables we refer to Planck Collaboration (2014b) and report here only the final formulas for the integrated Compton y -profile, Y_{500} ,

$$E^{-\beta}(z) \left[\frac{D_A^2(z) Y_{500}}{10^{-4} \text{ Mpc}} \right] = Y_* \left[\frac{h}{0.7} \right]^{-2+\alpha} \left[\frac{(1-b)M_{500}}{6 \cdot 10^{14} M_\odot} \right]^\alpha \quad (13)$$

and for the cluster angular size

$$\theta_{500} = \theta_* \left[\frac{h}{0.7} \right]^{-2/3} \left[\frac{(1-b)M_{500}}{3 \cdot 10^{14} M_\odot} \right]^{1/3} E^{-2/3}(z) \left[\frac{D_A(z)}{500 \text{ Mpc}} \right]^{-1} \quad (14)$$

In equations (13) and (14) $D_A(z)$ is again the angular diameter distance, h is the reduced Hubble constant, $H_0/100$,

and $E(z) = H(z)/H_0$. For the coefficients we follow what is reported in Planck Collaboration (2016e) and consider $\theta_* = 6.997 \text{ arcmin}$, $\beta = 0.66$ and for the others coefficients we use Gaussian distributed priors, reported in table 1. Equation (13) is derived with a dispersion, $\sigma_{\ln Y_*}$, given in table 1. We consider it as a nuisance parameter for the counts only, since its effect on the power spectrum amplitude is negligible (lower than 1%). Therefore we neglect the last term in Eq. (8).

The quantity b is defined as the mass bias and it takes into account the difference between the cluster mass estimation, obtained assuming hydrostatic equilibrium, and the real cluster mass. By following the Planck Collaboration (2016e) baseline, we use in this analysis a Gaussian distributed prior for $(1-b)$, from the Canadian Cluster Comparison Project (Hoekstra et al. 2015, labelled CCCP form now on), reported in table 1.

Parameter	Gaussian prior
$\log Y_*$	-0.19 ± 0.02
α	1.79 ± 0.08
$\sigma_{\ln Y_*}$	0.173 ± 0.023
$(1-b)$ CCCP	0.780 ± 0.092

Table 1. Priors on nuisance parameters for scaling relations, as defined in Planck Collaboration (2016e).

2.3.2. Mass function

In order to evaluate the theoretical mass function, we rely on numerical N -body simulations. In particular, for our analysis we use the mass function provided by Tinker et al. (2008). Therefore the number of halos per unit volume is given by

$$\frac{dN}{dM_{500}} = f(\sigma) \frac{\rho_{m,0}}{M_{500}} \frac{d \ln \sigma^{-1}}{dM_{500}}, \quad (15)$$

where $\rho_{m,0}$ is the matter density at redshift $z = 0$ and

$$f(\sigma) = A \left[1 + \left(\frac{\sigma}{b} \right)^{-a} \right] \exp \left(-\frac{c}{\sigma^2} \right). \quad (16)$$

In Eqs. (15) and (16), σ is the standard deviation of density perturbations in a sphere of radius $R = (3M/4\pi\rho_{m,0})^{1/3}$, calculated in linear regime, and it is given by

$$\sigma^2 = \frac{1}{2\pi^2} \int dk k^2 P(k, z) |W(kR)|^2, \quad (17)$$

where $W(kR)$ is the window function of a spherical top-hat of radius R .

We have evaluated the coefficients A , a , b and c in eq. (16) by interpolating the results provided by Tinker et al. (2008) at the required overdensity (i.e. $500 \rho_c(z)$).

3. Method

In this work, we constrain the cosmological parameters from galaxy clusters, exploiting the combination of number counts and power spectrum. We consider the cluster sample provided by [Planck Collaboration \(2016f\)](#), which consists of 439 clusters from the 65% cleanest part of the sky, above the signal-to-noise ratio threshold of 6 and in the redshift range $z = [0, 1]$. In order to obtain the cluster number counts, we sample both on redshift and on signal-to-noise ratio bins, as described in [Planck Collaboration \(2016e\)](#). For the power spectrum, we use Planck estimates from [Planck Collaboration \(2016d\)](#) and an estimate of the angular power spectrum from SPT at $\ell = 3000$ ([George et al. 2015](#)). We integrate in the redshift range $z = [0, 3]$ and in the mass range $M_{500} = [10^{13} h^{-1} M_{\odot}, 5 \cdot 10^{15} h^{-1} M_{\odot}]$, following [Planck Collaboration \(2016d\)](#). In combining cluster number counts and tSZ power spectrum, we follow the analysis shown in [Hurier & Lacasa \(2017\)](#) and neglect any correlations between the two probes.

We use a Monte Carlo Markov Chains (MCMC) approach to sample and constrain at the same time cosmological and scaling-relation parameters, that we consider as nuisance parameters in this analysis. We stress that even if SZ number counts and power spectrum show similar dependences on cosmological parameters, they have different dependences on scaling relations parameters. We find $dN/dz \propto \sigma_8^9 \Omega_m^3 (1-b)^{3.6}$ and $C_{\ell}^{\text{tSZ}} \propto \sigma_8^{8.1} \Omega_m^{3.2} (1-b)^{0.6}$. Combining the two probes, we should therefore be able to reduce the degeneracy between nuisance and cosmological parameters.

For the present analysis, we use the November 2016 version of the publicly available package `cosmomc` ([Lewis & Bridle 2002](#)), relying on a convergence diagnostic based on the Gelman and Rubin statistic. This version includes the cluster number-count likelihood for Planck ([Planck Collaboration 2016e](#)). We modify it to add the likelihood for the tSZ power spectrum ([Planck Collaboration 2014c](#)).

For the cosmological model, we first consider the Λ CDM model, varying the six standard parameters: Baryon and cold dark matter densities ω_b and ω_c , ratio of the sound horizon to the angular diameter distance at decoupling θ , scalar spectral index n_s , overall normalization of the spectrum A_s at $k = 0.05 \text{ Mpc}^{-1}$, and reionization optical depth τ . We update the results from [Planck Collaboration \(2016c\)](#) with the new value of the optical depth from [Planck Collaboration \(2016g,h\)](#) by adding a Gaussian prior in our analysis, i.e. $\tau = 0.055 \pm 0.009$. We include in our analysis the four scaling parameters reported in table 1, i.e. Y_* , α , $(1-b)$ and $\sigma_{\ln Y_*}$ for number counts only. Since SZ number counts and power spectrum are not able to constrain the basic six-parameters model alone, we add also BAO measurements from [Anderson et al. \(2014\)](#). We compare and combine our results with CMB primary temperature and polarisation anisotropies data from [Planck Collaboration \(2016c\)](#), updated with the new optical depth reported above.

Finally, we explore results obtained by relaxing the assumptions of the standard model, i.e. allowing first the sum of neutrino masses $\sum m_{\nu}$ and then the dark energy EoS parameter w to vary, and therefore adding them to our analysis.

4. Results

We report here our results, comparing constraints from tSZ power spectrum alone, tSZ number counts alone and their combination. We compare these results with the ones obtained from CMB temperature and polarization anisotropy data and the complete combination of datasets (power spectrum, number counts and CMB data). We analyse both standard Λ CDM model and extensions to it.

We present results for cosmological parameters to which galaxy clusters are more sensitive, in particular the total matter density, Ω_m , and the standard deviation of density perturbations, defined in Eq. (17), evaluated at radius $R = 8 \text{ Mpc } h^{-1}$, σ_8 .

4.1. Λ CDM model

We first show the effect of the new value of the optical depth. In Fig. 1, we compare two-dimensional probability distributions for τ and σ_8 for tSZ number counts and CMB data, for the different values of τ . We find that, while this change in the optical depth does not affect the constraining power of cluster number counts on σ_8 , it modifies constraints from CMB, reducing therefore the discrepancy between the two different probes. The change in CMB constraints is due to the degeneracy between optical depth and σ_8 , i.e. the fact the small-scale CMB power spectrum is proportional to the quantity $\sigma_8 e^{-\tau}$ (see e.g., [Planck Collaboration 2014a](#)). The improved constraint on σ_8 from CMB reduces the tension with SZ number counts from 2.4σ ([Planck Collaboration 2016c](#)) to 1.5σ .

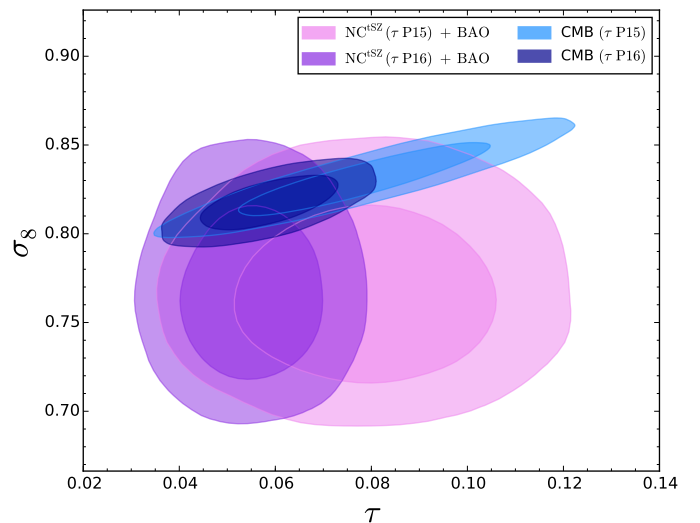


Fig. 1. Two dimensional probability distributions for τ and σ_8 for different values of optical depths (see text). We compare results for SZ number counts only (pink and purple) and for CMB data only (blue and light blue).

We focus now on the results for σ_8 and the matter density Ω_m . We show the constraints from CMB temperature and polarization anisotropies data, from the tSZ power spectrum alone (C_{ℓ}^{tSZ}), from tSZ number counts alone (NC^{tSZ}), from the combination of the two tSZ probes ($C_{\ell}^{\text{tSZ}} + \text{NC}^{\text{tSZ}}$) and finally those from the complete combination of all datasets (CMB + $C_{\ell}^{\text{tSZ}} + \text{NC}^{\text{tSZ}}$), adding also BAO data. We stress that from now on we always use the

new prior for the optical depth and that results for C_ℓ^{tSZ} are always obtained by combining Planck and SPT data. We display the results in Fig. 2 and we summarize the constraints (68% c.l.) in Tab. 3 for the different datasets.

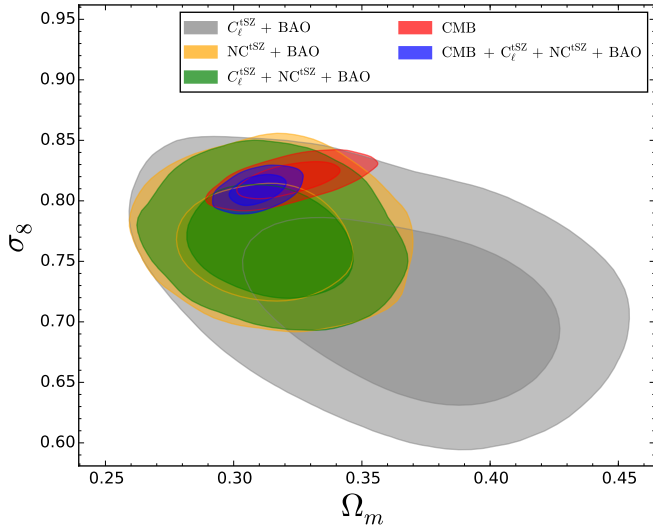


Fig. 2. Two dimensional probability distributions for Ω_m and σ_8 in the Λ CDM scenario, for power spectrum only (grey), number counts only (orange), the combination of the two probes (green), CMB only (red) and the combination of all the probes (blue).

When considering the combination of tSZ number counts and power spectrum, we note that the combination is driven by tSZ counts since tSZ spectrum shows weaker constraints (see comparison of the Figure of Merits (FoM) for the different datasets in Tab. 2). We nevertheless obtain a small improvement on the Ω_m and σ_8 constraints, within 10% on individual error bars. The slight differences in scaling-cosmological parameter degeneracies between the two tSZ probes drive this small improvement, as shown in Fig. 4. As of the comparison between constraints from CMB and from tSZ combined probes, we find a discrepancy similar to the case of CMB vs tSZ counts alone, of $\simeq 1.6\sigma$.

We now focus on the scaling-relation parameters and in particular on the mass bias, which significantly affects the values of σ_8 . As noted in Planck Collaboration (2014b, 2016e), low values of mass bias lead to large values of σ_8 (see also Fig. 4). We display in Fig. 3 the results from the tSZ combination probes, and adding CMB data, together with the CCCP-based prior considered in our analysis. In our updated analysis with the new optical depth, we find that results from the tSZ combined probes are driven by the prior distribution. Adding CMB data to the tSZ counts or to the combined tSZ probes drives the mass bias to lower values (not adding BAO data in this case, in order to fully compare with results from Planck Collaboration (2016e)). On the one hand, we find that the bias needed to reconcile CMB constraints with those from the tSZ number counts is $(1-b) = 0.62 \pm 0.07$, comparable to the value $(1-b) = 0.58 \pm 0.04$ found in Planck Collaboration (2016e). On the other hand, the bias increases to $(1-b) = 0.64 \pm 0.04$ when using the tSZ counts and power spectrum.

FoM	C_ℓ^{tSZ}	NC^{tSZ}	$C_\ell^{\text{tSZ}} + \text{NC}^{\text{tSZ}}$
1	560	1462	1744
$\sigma_{\sigma_8} \sigma_{\Omega_m}$			

Table 2. Figures of Merit (FoM) for tSZ spectrum only, number counts only and the combination of the two probes, for Ω_m and σ_8 parameters in Λ CDM scenario.

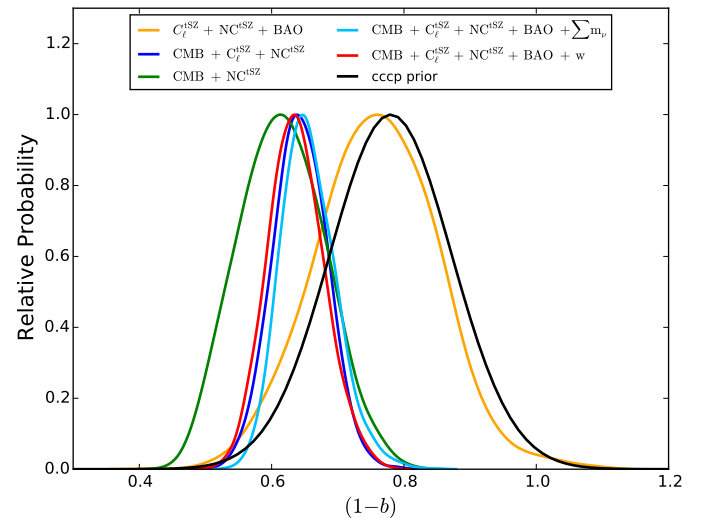


Fig. 3. One dimensional probability distribution for the mass bias $(1-b)$ for different dataset combinations: the complete tSZ combination and BAO (orange); CMB and the complete tSZ combination (blue); CMB and number counts (green); the combination of CMB and tSZ, adding the effect of massive neutrinos (lightblue); the combination of CMB and tSZ, adding the effect of varying the dark energy EoS parameter (red). All are compared to the CCCP prior we have used in our analysis (black).

4.2. Extensions to Λ CDM

We now consider two extensions to Λ CDM model: adding massive neutrinos and including the Equation of State (EoS) of dark energy. For these extensions to the standard model, we explore whether the combination of the two tSZ probes can improve the constraints on cosmological and scaling-relation parameters, with respect to number counts only. We compare these different results with constraints from CMB only and from the complete combination of all datasets.

4.2.1. Massive neutrinos

Adding massive neutrinos damps the amplitude of matter power spectrum at small scales which in turn lowers the value of σ_8 . We present in Fig. 5 and in Tab. 4 the new constraints on Ω_m and σ_8 obtained from number counts alone, from CMB alone, from tSZ probes alone, and from the combination of the three. Constraints from CMB primary anisotropies alone worsen, as compared to the Λ CDM case, because of the low sensitivity of CMB to the neutrino mass. As expected, lower values of σ_8 are reached, but along a $\Omega_m - \sigma_8$ degeneracy line, parallel to the tSZ one.

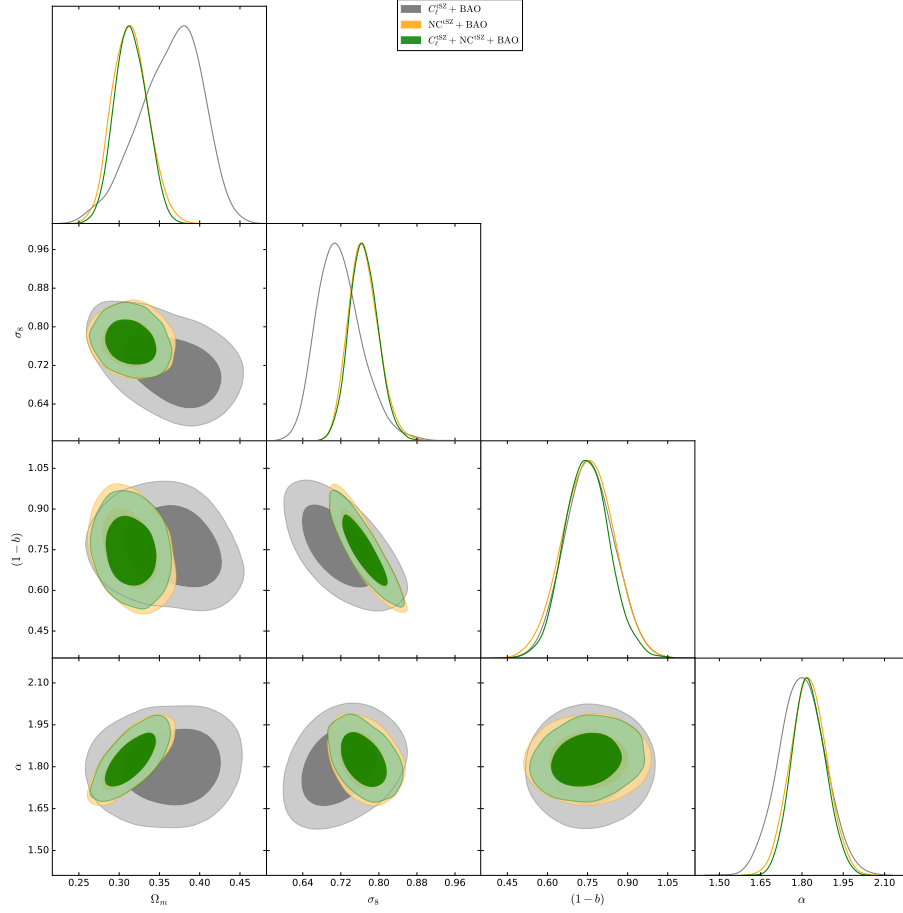


Fig. 4. Correlation between cosmological and scaling-relation parameters in the case of tSZ power spectrum (grey), number counts (orange) and for the combination of both (green).

Cosmological parameters	$C_\ell^{\text{tSZ}} + \text{BAO}$	$\text{NC}^{\text{tSZ}} + \text{BAO}$	$C_\ell^{\text{tSZ}} + \text{NC}^{\text{tSZ}} + \text{BAO}$	CMB	CMB + $C_\ell^{\text{tSZ}} + \text{NC}^{\text{tSZ}} + \text{BAO}$
Ω_m	$0.363^{+0.046}_{-0.032}$	$0.314^{+0.020}_{-0.024}$	0.315 ± 0.020	$0.321^{+0.012}_{-0.014}$	0.309 ± 0.007
σ_8	$0.719^{+0.037}_{-0.055}$	$0.768^{+0.028}_{-0.035}$	$0.769^{+0.028}_{-0.032}$	0.817 ± 0.010	0.809 ± 0.008
$S_8 = \sigma_8(\Omega_m/0.3)^{1/3}$	$0.764^{+0.040}_{-0.050}$	$0.780^{+0.029}_{-0.042}$	$0.781^{+0.028}_{-0.034}$	0.836 ± 0.018	0.818 ± 0.012
Nuisance parameters	$C_\ell^{\text{tSZ}} + \text{BAO}$	$\text{NC}^{\text{tSZ}} + \text{BAO}$	$C_\ell^{\text{tSZ}} + \text{NC}^{\text{tSZ}} + \text{BAO}$	CMB	CMB + $C_\ell^{\text{tSZ}} + \text{NC}^{\text{tSZ}} + \text{BAO}$
$(1-b)$	0.758 ± 0.090	0.754 ± 0.093	$0.748^{+0.080}_{-0.081}$	-	$0.649^{+0.034}_{-0.037}$
α	1.801 ± 0.081	1.824 ± 0.064	$1.825^{+0.057}_{-0.063}$	-	$1.788^{+0.035}_{-0.039}$
$\log Y_*$	-0.188 ± 0.021	-0.189 ± 0.020	-0.189 ± 0.021	-	-0.194 ± 0.020
$\sigma_{\ln Y_*}$	-	0.075 ± 0.010	0.075 ± 0.010	-	0.075 ± 0.010

Table 3. 68% c.l. constraints for cosmological and scaling-relation parameters in the Λ CDM scenario, from power spectrum (C_ℓ^{tSZ}) and number counts (NC^{tSZ}) alone and for the combination of the two probes ($C_\ell^{\text{tSZ}} + \text{NC}^{\text{tSZ}}$). We compare these results with constraints from CMB primary anisotropies and from the complete combination of datasets.

Constraints from tSZ probes alone are not significantly affected by the neutrino mass. As a matter of fact the high S/N threshold of the Planck cluster sample selects massive clusters ($M \gtrsim 2. \times 10^{14}$) which abundance is not impacted by matter power-spectrum damping. As for the Planck tSZ power spectrum, it does not probe sufficiently

well the small angular scales where the effect of the matter power-spectrum damping due to massive neutrinos should take place. However, the addition of estimation of the tSZ power spectrum at $\ell = 3000$ from SPT is expected to increase the sensitivity of the power spectrum to massive neutrinos. The full tSZ probe combination thus improves the

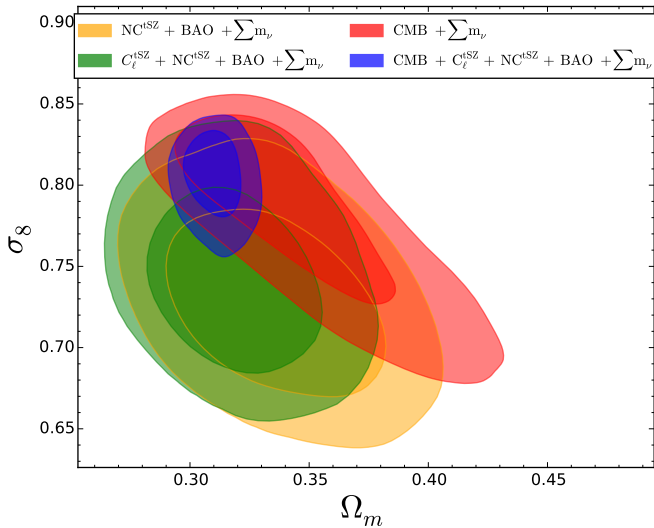


Fig. 5. Two dimensional probability distributions for Ω_m and σ_8 for varying neutrino mass scenario. We report in orange results from number counts, in green the combination of number counts and power spectrum, we add also CMB data (blue) and we show results for CMB only (red).

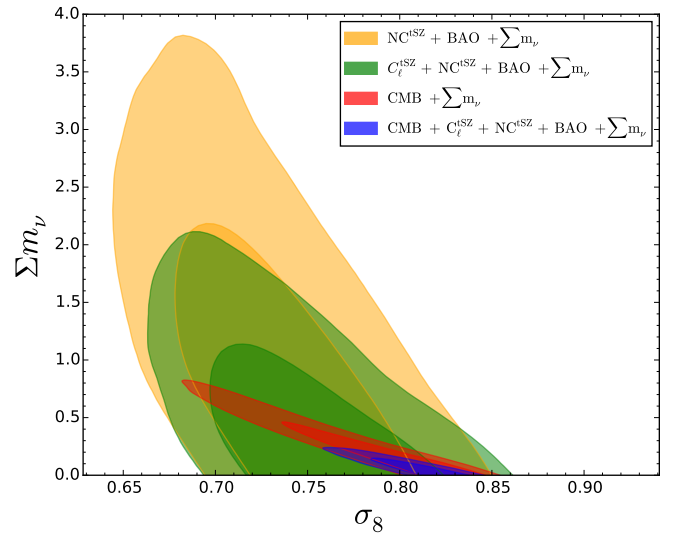


Fig. 6. Two dimensional probability distributions for σ_8 and $\sum m_\nu$ for varying neutrino mass scenario. We report results for number counts (orange), the combination of number counts and power spectrum (green), we add also CMB data (blue) and we show results for CMB only (red).

final constraints on cosmological parameters with respect to number counts only, as can be seen in Figs. 5 and 6 and in Tab. 4. In particular, it provides an upper 95% limit on neutrino mass $\sum m_\nu < 1.53$ eV, while number counts alone are only able to provide $\sum m_\nu < 2.83$ eV.

The constraints from the combination between tSZ probes and CMB are mainly driven by the latter, as can be seen in Figs. 5 and 6. Despite the wider CMB constraints along the degeneracy line, we obtain an agreement within 1.2σ between CMB and the tSZ probes. We show the results from the combination of tSZ probes and the CMB data with massive neutrinos as the light blue line in Fig. 3. The preferred bias value is $(1 - b) = 0.66 \pm 0.04$, of the same order of the Λ CDM case. Finally, we find an upper limit on the neutrino mass of $\sum m_\nu < 0.19$ eV at 95%, slightly more stringent than constraints obtained from CMB alone ($\sum m_\nu < 0.49$ eV, from Planck Collaboration (2016c)).

4.2.2. Dark energy EoS

We now consider the extension of the parameter space to dark energy EoS by allowing it to differ from the standard value $w = -1$ for a cosmological constant. We focus on the simplest case where w is constant with time. We show the constraints on matter density Ω_m and σ_8 in Fig. 7 and Tab. 5. Again, CMB constraints are enlarged along a degeneracy line but towards higher values of σ_8 and lower values of Ω_m . We find a discrepancy between CMB and tSZ probes, at about 2.4σ and it is still driven by the σ_8 parameter, as shown in Fig. 8. For the combination of tSZ probes we find a value of EoS parameter $w = -1.00^{+0.18}_{-0.17}$ (68% c.l.), consistent with the one found in Planck Collaboration (2016e) ($w = -1.01 \pm 0.18$ for number counts in combination with BAO). We underline that in this case, as for the Λ CDM scenario, the addition of tSZ power spectrum does not improve the results with respect to number counts only. Therefore we decide to show only the tSZ combination in Figs. 7 and 8, reporting all the results in Tab. 5. For the complete

combination of CMB and tSZ, we find the 68% constraints $w = -1.04^{+0.08}_{-0.06}$. We stress that these results (both for tSZ probes alone and in combination with CMB data) present a 1σ consistency with the standard value $w = -1$, while results from CMB and BAO reported in Planck Collaboration (2016e) show only a 2σ consistency. Given the very good agreement with the standard value of EoS parameter, we choose not to investigate other possible parameterisations in this analysis.

Finally, we stress that also in this case the preferred value of the mass bias for the complete combination of CMB and tSZ probes is shifted to lower values, $(1 - b) = 0.64 \pm 0.04$, as shown also in Fig. 3, red line.

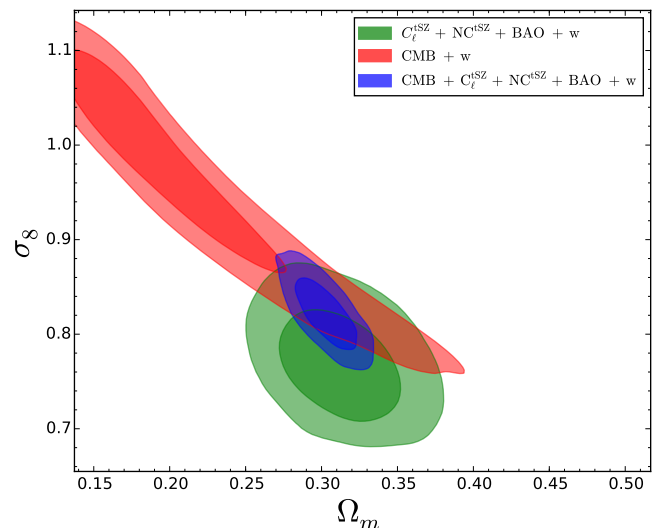


Fig. 7. Two dimensional probability distributions for Ω_m and σ_8 for varying dark energy EoS scenario, for the combination of number counts and power spectrum (green), the addition of CMB data (blue) and for CMB only (red).

Cosmological parameters	NC ^{tSZ} + BAO	$C_\ell^{\text{tSZ}} + \text{NC}^{\text{tSZ}} + \text{BAO}$	CMB	CMB + $C_\ell^{\text{tSZ}} + \text{NC}^{\text{tSZ}} + \text{BAO}$
Ω_m	$0.336^{+0.027}_{-0.031}$	$0.321^{+0.020}_{-0.023}$	$0.345^{+0.020}_{-0.038}$	$0.310^{+0.007}_{-0.008}$
σ_8	$0.729^{+0.033}_{-0.039}$	$0.745^{+0.031}_{-0.040}$	$0.783^{+0.052}_{-0.024}$	$0.805^{+0.021}_{-0.012}$
$S_8 = \sigma_8(\Omega_m/0.3)^{1/3}$	$0.757^{+0.029}_{-0.040}$	$0.762^{+0.028}_{-0.042}$	$0.819^{+0.031}_{-0.024}$	$0.814^{+0.020}_{-0.015}$
$\sum m_\nu$	$< 2.83 \text{ eV}$	$< 1.53 \text{ eV}$	$< 0.65 \text{ eV}$	$< 0.19 \text{ eV}$
Nuisance parameters	NC ^{tSZ} + BAO	$C_\ell^{\text{tSZ}} + \text{NC}^{\text{tSZ}} + \text{BAO}$	CMB	CMB + $C_\ell^{\text{tSZ}} + \text{NC}^{\text{tSZ}} + \text{BAO}$
$(1 - b)$	0.749 ± 0.091	$0.760^{+0.096}_{-0.088}$	-	$0.657^{+0.036}_{-0.047}$
α	1.788 ± 0.076	$1.792^{+0.070}_{-0.064}$	-	$1.791^{+0.036}_{-0.040}$
$\log Y_*$	-0.191 ± 0.020	0.190 ± 0.020	-	-0.195 ± 0.020
$\sigma_{\ln Y_*}$	0.075 ± 0.010	0.075 ± 0.010	-	0.074 ± 0.010

Table 4. 68% c.l. constraints for cosmological and scaling-relation parameters and 95% upper limits for neutrino mass for varying neutrino mass scenario, from number counts (NC^{tSZ}), the combination of power spectrum and number counts ($C_\ell^{\text{tSZ}} + \text{NC}^{\text{tSZ}}$), the addition of CMB data (CMB + $C_\ell^{\text{tSZ}} + \text{NC}^{\text{tSZ}}$) and for CMB alone.

Cosmological parameters	NC ^{tSZ} + BAO	$C_\ell^{\text{tSZ}} + \text{NC}^{\text{tSZ}} + \text{BAO}$	CMB	CMB + $C_\ell^{\text{tSZ}} + \text{NC}^{\text{tSZ}} + \text{BAO}$
Ω_m	$0.315^{+0.025}_{-0.028}$	$0.313^{+0.023}_{-0.027}$	$0.209^{+0.023}_{-0.071}$	0.303 ± 0.013
σ_8	$0.769^{+0.032}_{-0.041}$	$0.770^{+0.031}_{-0.041}$	$0.969^{+0.109}_{-0.057}$	0.822 ± 0.024
$S_8 = \sigma_8(\Omega_m/0.3)^{1/3}$	$0.781^{+0.030}_{-0.042}$	$0.780^{+0.029}_{-0.040}$	0.846 ± 0.020	$0.824^{+0.017}_{-0.019}$
w	$-1.01^{+0.20}_{-0.17}$	$-1.00^{+0.18}_{-0.17}$	$-1.56^{+0.21}_{-0.40}$	$-1.041^{+0.080}_{-0.063}$
Nuisance parameters	NC ^{tSZ} + BAO	$C_\ell^{\text{tSZ}} + \text{NC}^{\text{tSZ}} + \text{BAO}$	CMB	CMB + $C_\ell^{\text{tSZ}} + \text{NC}^{\text{tSZ}} + \text{BAO}$
$(1 - b)$	0.750 ± 0.091	$0.751^{+0.096}_{-0.089}$	-	$0.637^{+0.040}_{-0.045}$
α	1.828 ± 0.067	1.819 ± 0.060	-	1.780 ± 0.040
$\log Y_*$	-0.189 ± 0.021	-0.180 ± 0.021	-	-0.194 ± 0.021
$\sigma_{\ln Y_*}$	0.075 ± 0.010	0.075 ± 0.010	-	0.074 ± 0.010

Table 5. 68% c.l. constraints for cosmological and scaling-relation parameters for varying dark energy EoS scenario, from number counts (NC^{tSZ}), the combination of power spectrum and number counts ($C_\ell^{\text{tSZ}} + \text{NC}^{\text{tSZ}}$), the addition of CMB data (CMB + $C_\ell^{\text{tSZ}} + \text{NC}^{\text{tSZ}}$) and for CMB alone.

5. Discussion

The tSZ cluster counts and CMB tension reported in [Planck Collaboration \(2016e\)](#), in agreement with constraints obtained independently from the tSZ power spectrum, 1D pdf, and bispectrum ([Planck Collaboration 2016d](#)), has triggered a lot of interest in the community. On the one hand, multiple estimates of the cluster masses were performed to investigate whether this discrepancy could be attributed to the mass bias (see Fig. 10 for a summary of some of the most recent estimates). On the other hand, multiple cosmological analyses were performed to investigate the CMB/LSS tension or to try to reduce it.

In this study, we provide constraints on cosmological parameters, considering as a baseline the updated value

of the optical depth from [Planck Collaboration \(2016g\)](#), $\tau = 0.055 \pm 0.009$ and including the SPT high multipole tSZ spectrum estimate ([George et al. 2015](#)). The new value of τ modifies the results from CMB primary anisotropies, increasing the constraining power on σ_8 of about 1σ . This is due to the dependence of CMB power spectrum small scale regime to the combination $\sigma_8 e^{-\tau}$. Results on σ_8 from number counts remain unchanged, given that we use the approach and cluster sample from [Planck Collaboration \(2016c\)](#). For the tSZ effect, we assume the same baseline model than the one of [Planck Collaboration \(2016e\)](#), i.e. we use a mass function from [Tinker et al. \(2008\)](#) and a Gaussian prior on mass bias from [Hoekstra et al. \(2015\)](#), in agreement with the average mass bias obtained from the recent weak lensing (WL) estimates (Fig. 10). In this way,

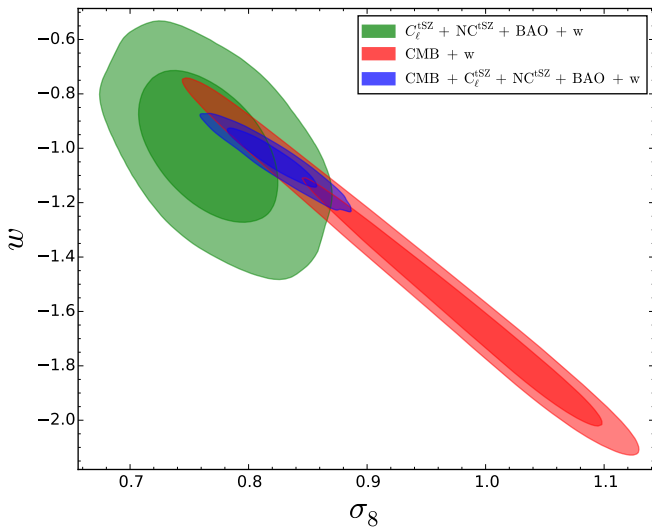


Fig. 8. Two dimensional probability distributions for σ_8 and w for varying dark energy EoS scenario, for the combination of number counts and power spectrum (green), the addition of CMB data (blue) and for CMB only (red).

we can more easily and directly compare with results from [Planck Collaboration \(2016e\)](#).

The changes in the CMB results when considering the new value of τ reduce the discrepancy with tSZ counts, i.e. from 2.4σ to 1.5σ in the present study. We perform an actual combined analysis of tSZ number counts and power spectrum, in order to carry on a complete MCMC exploration of the parameter space, sampling at the same time on cosmological and scaling-relation parameters. We neglect the correlation between the two combined probes in the likelihood as it is expected to be low with current Planck cluster sample and large scale power spectrum estimate ([Hurier & Lacasa 2017](#)). We find that the addition of tSZ power spectrum (including Planck and SPT) leads to 1.6σ tension on σ_8 when compared to CMB results. Recent studies using the LSS probes seem to also show a disagreement with CMB's best cosmology: based on clusters samples [Vikhlinin et al. \(2009\)](#); [Hasselfield et al. \(2013\)](#); [Benson et al. \(2013\)](#); [Böhringer & Chon \(2016\)](#); [Böhringer et al. \(2017\)](#), on the linear growth rate data ([Moresco & Marulli 2017](#), and references therein), or on cosmic shear ([Hildebrandt et al. 2017](#); [van Uitert et al. 2017](#); [Joudaki et al. 2017](#)). Despite intrinsic limitations to each of these probes (e.g. [Efsthathiou & Lemos \(2017\)](#)), the LSS cosmological analyses exhibit a general trend towards lower values of σ_8 .

It was noticed in [Planck Collaboration \(2016e\)](#) that there was a factor ~ 2.5 more clusters predicted than observed when taking into account the CMB cosmology and a mass bias of 0.8. The new optical depth reduces the σ_8 derived from the CMB analysis to $\sigma_8 = 0.817 \pm 0.018$. Nevertheless, assuming a mass bias of 0.8 (average value of recent WL estimates), due to the large value of σ_8 , we still find a difference between predicted and observed low redshift ($z < 0.3$) cluster number counts of the order of 2.5 (Fig. 9).

More biased estimates of the cluster mass could explain this difference, and in turn reduce the tSZ/CMB tension since cosmological parameters are degenerate with scaling-

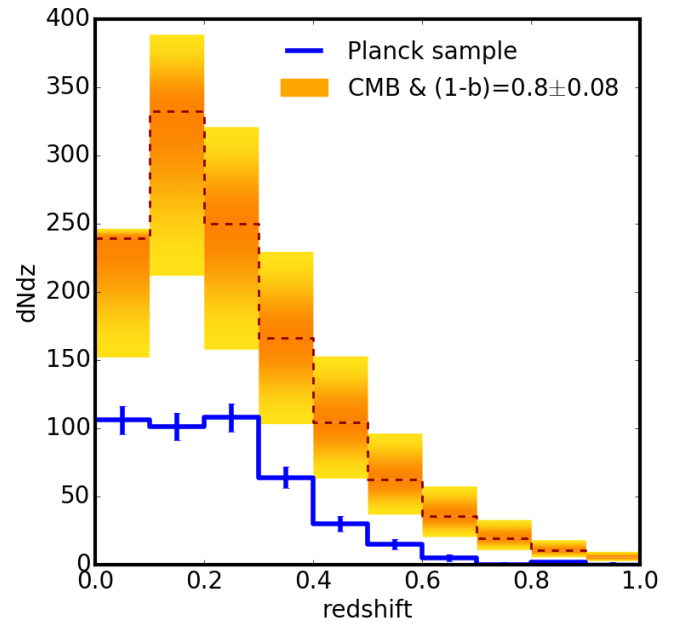


Fig. 9. tSZ cluster sample from Planck (blue line) compared with predicted counts with CMB best-fit cosmological parameters and $(1-b) = 0.8 \pm 0.08$ (red line and orange envelope).

relation parameters. We thus focus on the mass bias $(1-b)$. We show results for the combination of CMB primary anisotropies and number counts and the complete combination of CMB and tSZ probes, all using the updated value of the optical depth. For the first case, we find a low value for the mass bias $(1-b) = 0.62 \pm 0.07$, fully consistent with results from [Planck Collaboration \(2016e\)](#), while for the latter case, the addition of tSZ power spectrum data increases the bias of about 2σ with respect to [Planck Collaboration \(2016e\)](#). This leads to $(1-b) = 0.66 \pm 0.04$. Hydrostatic mass estimates from X-ray observations (used to derive the scaling relation of Eq. 13) are known to be biased low from numerical simulation but by not more than 20% ([Lau et al. \(2013\)](#); [Biffi et al. \(2016\)](#) and a compilation of comparisons in [Planck Collaboration \(2014b\)](#), purple area in Fig. 10). With higher number of high resolution optical observations of cluster samples and improved weak lensing mass measurements, many comparisons were made between X-ray or tSZ masses and WL masses. Assuming that WL reconstruction provides unbiased estimates of the true mass, many teams derived bias estimates (e.g. [Medezinski et al. 2017](#); [Serenio et al. 2017](#); [Jimeno et al. 2017](#); [Parroni et al. 2017](#); [Okabe & Smith 2016](#); [Battaglia et al. 2016](#); [Applegate et al. 2016](#); [Smith et al. 2016](#); [Hoekstra et al. 2015](#); [Simet et al. 2015](#); [Israel et al. 2015](#); [von der Linden et al. 2014](#); [Donahue et al. 2014](#); [Gruen et al. 2014](#); [Mahdavi et al. 2013](#), shown as black dots, from top to bottom, in Fig. 10). These biases average around a value of $(1-b) \sim 0.8 \pm 0.08$, with one low mass bias estimated in [von der Linden et al. \(2014\)](#).

As seen in Fig. 10, where we plot the largest mass bias possibly obtained from our combined analysis, we find values of $(1-b)$ that do not agree with those derived from numerical simulations and observations. Moreover, reducing the SZ-CMB tension by allowing smaller values of $(1-b)$ seems to be not sufficient for alleviating the global differ-

ence between low- z - and high- z -based cosmological parameters. Another possibility to reconcile CMB and tSZ is to relax some assumptions of the standard model. In particular, we find $(1 - b) = 0.66 \pm 0.04$ when adding massive neutrinos and $(1 - b) = 0.64 \pm 0.04$ when opening the parameter space to a varying EoS parameter. This implies that, even exploring extension to Λ CDM, the complete combination of CMB and tSZ probes still points towards low values of $(1 - b)$ and does not allow us to fully reconcile the probes.

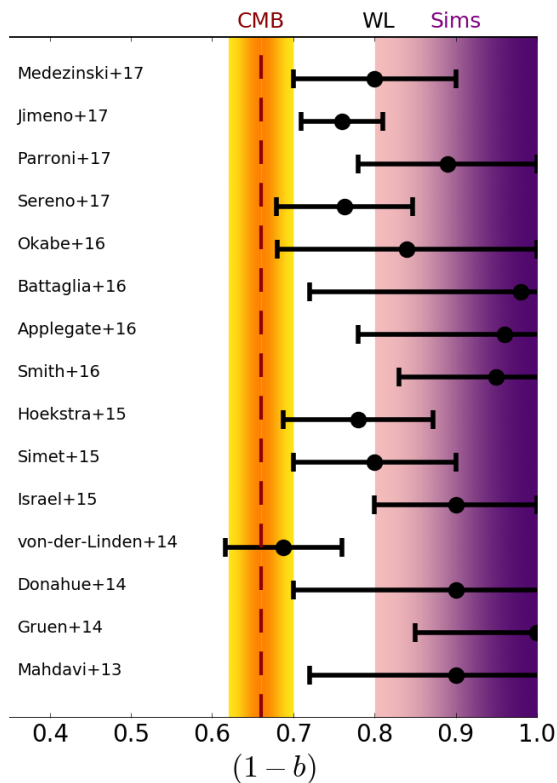


Fig. 10. Comparison of estimates of the mass bias from combined Λ CDM SZ and CMB analysis, WL-hydrostatic mass ratio and simulations. (See text for references to the mass bias estimates from the WL analyses.)

As of today, the cluster number counts are not suffering from statistical uncertainty but are rather limited by systematic effects, mainly the mass estimates. The tSZ power spectrum, in turn, is not measured with sufficient accuracy, especially at small angular scales, to reduce the tension with CMB. The tSZ cosmological analysis can be improved by considering more realistic and complex hypotheses on the mass bias (e.g. redshift and/or mass dependence), the pressure profile and the mass function. It can also be improved by refining the likelihood analysis, such as including correlations between probes, missing or inaccurate redshifts (e.g. [Bonaldi et al. \(2014\)](#)) and additional tSZ probes (e.g. bispectrum [Hurier & Lacasa \(2017\)](#)).

6. Conclusion

We update the constraints on cosmological parameters from tSZ cluster counts and power spectrum, using the most recent optical depth value from Planck and performing a combined analysis of the two probes, adding also CMB data.

In the Λ CDM case, we find that the combined analysis of tSZ counts and power spectrum improves slightly the accuracy on Ω_m and σ_8 constraints and leads to a discrepancy of almost 1.6σ on σ_8 when compared to CMB results.

We then consider the effect of massive neutrinos, finding that the combination of tSZ counts and power spectrum allows us to obtain an upper limit on the neutrino mass, $\sum m_\nu < 1.53$ eV, resulting in an improvement of almost a factor 2 compared to number counts only. Despite being weak as compared to other cosmological probes, tSZ data alone provide us with an independent constraint that can be combined in particular with CMB. In this case, the combination of tSZ probes and CMB leads a 95% upper limit on massive neutrinos of $\sum m_\nu < 0.19$ eV. Moreover due to the enlargement of CMB constraints, we find that CMB results and combined tSZ results on σ_8 agree within 1.2σ . When we allow the EoS parameter w for the dark energy to vary, the tSZ and CMB still show a 2.4σ discrepancy on σ_8 . The full combination of probes provides $w = -1.04 \pm 0.07$ consistent with the standard $w = -1$ value.

Finally, we find that the complete combination of tSZ probes and CMB data points towards low values of the mass bias (almost 2σ discrepancy) with respect to simulations and to other tracers of large scale structure. Such a difference between mass estimates implies that, regardless of the CMB/LSS tension, a better understanding of the intrinsic systematic effects and differences between probes is needed.

Acknowledgements. LS acknowledges support from the grant "Borsa di studio di perfezionamento all'estero" from University of Rome, Sapienza and "Fondazione Angelo della Riccia". Based on observations obtained with Planck (<http://www.esa.int/Planck>), an ESA science mission with instruments and contributions directly funded by ESA Member States, NASA, and Canada. This project has received funding from the European Research Council (ERC) under the European Union's Horizon 2020 research and innovation programme grant agreement ERC-2015-AdG 695561.

References

- Allen, S. W., Evrard, A. E., & Mantz, A. B. 2011, *Ann. Rev. Astron. Astrophys.*, 49, 409
- Anderson, L. et al. 2014, *Mon. Not. Roy. Astron. Soc.*, 441, 24
- Applegate, D. E., Mantz, A., Allen, S. W., et al. 2016, *MNRAS*, 457, 1522
- Arnaud, M., Pratt, G. W., Piffaretti, R., et al. 2010, *Astron. Astrophys.*, 517, A92
- Battaglia, N., Leauthaud, A., Miyatake, H., et al. 2016, *J. Cosmology Astropart. Phys.*, 8, 013
- Benson, B. A., de Haan, T., Dudley, J. P., et al. 2013, *ApJ*, 763, 147
- Biffi, V., Borgani, S., Murante, G., et al. 2016, *ApJ*, 827, 112
- Bleem, L. E. et al. 2015, *Astrophys. J. Suppl.*, 216, 27
- Boehringer, H., Chon, G., Retzlaff, J., et al. 2017, *Astron. J.*, 153, 220
- Böhringer, H. & Chon, G. 2016, *Modern Physics Letters A*, 31, 1640008
- Böhringer, H., Chon, G., Retzlaff, J., et al. 2017, *AJ*, 153, 220
- Bonaldi, A., Battye, R., & Brown, M. L. 2014, *Astrophys. J.*, 786, 88
- Chon, G. & Böhringer, H. 2012, *Astron. Astrophys.*, 538, A35
- Cooray, A. 2000, *Phys. Rev.*, D62, 103506
- Cooray, A. 2001, *Phys. Rev.*, D64, 063514
- Donahue, M., Voit, G. M., Mahdavi, A., et al. 2014, *ApJ*, 794, 136
- Efstathiou, G. & Lemos, P. 2017 [[arXiv:1707.00483](https://arxiv.org/abs/1707.00483)]
- George, E. M. et al. 2015, *Astrophys. J.*, 799, 177
- Gruen, D., Seitz, S., Brimiouille, F., et al. 2014, *MNRAS*, 442, 1507
- Hasselfield, M., Hilton, M., Marriage, T. A., et al. 2013, *J. Cosmology Astropart. Phys.*, 7, 008
- Hildebrandt, H., Viola, M., Heymans, C., et al. 2017, *MNRAS*, 465, 1454
- Hoekstra, H., Herbonnet, R., Muzzin, A., et al. 2015, *Mon. Not. Roy. Astron. Soc.*, 449, 685

- Horowitz, B. & Seljak, U. 2017, *Mon. Not. Roy. Astron. Soc.*, 469, 394
- Hurier, G. & Lacasa, F. 2017, *Astron. Astrophys.*, 604, A71
- Israel, H., Schellenberger, G., Nevalainen, J., Massey, R., & Reiprich, T. H. 2015, *MNRAS*, 448, 814
- Jimeno, P., Diego, J.-M., Broadhurst, T., De Martino, I., & Lazkoz, R. 2017, *ArXiv e-prints* [[arXiv:1706.00395](#)]
- Joudaki, S., Blake, C., Johnson, A., et al. 2017, *ArXiv e-prints* [[arXiv:1707.06627](#)]
- Komatsu, E. & Kitayama, T. 1999, *Astrophys. J.*, 526, L1
- Komatsu, E. & Seljak, U. 2002, *Mon. Not. Roy. Astron. Soc.*, 336, 1256
- Lau, E. T., Nagai, D., & Nelson, K. 2013, *Astrophys. J.*, 777, 151
- Lesgourgues, J. & Pastor, S. 2012, *Adv. High Energy Phys.*, 2012, 608515
- Lewis, A. & Bridle, S. 2002, *Phys. Rev.*, D66, 103511
- Mahdavi, A., Hoekstra, H., Babul, A., et al. 2013, *ApJ*, 767, 116
- Marriage, T. A. et al. 2011, *Astrophys. J.*, 737, 61
- Medezinski, E., Battaglia, N., Umetsu, K., et al. 2017, *ArXiv e-prints* [[arXiv:1706.00434](#)]
- Moresco, M. & Marulli, F. 2017, *ArXiv e-prints* [[arXiv:1705.07903](#)]
- Okabe, N. & Smith, G. P. 2016, *MNRAS*, 461, 3794
- Parroni, C., Mei, S., Erben, T., et al. 2017, *ArXiv e-prints* [[arXiv:1705.04329](#)]
- Planck Collaboration. 2014a, *A&A*, 571, A16
- Planck Collaboration. 2014b, *A&A*, 571, A20
- Planck Collaboration. 2014c, *A&A*, 571, A21
- Planck Collaboration. 2014d, *A&A*, 571, A29
- Planck Collaboration. 2016a, *A&A*, 594, A1
- Planck Collaboration. 2016b, *A&A*, 594, A11
- Planck Collaboration. 2016c, *A&A*, 594, A13
- Planck Collaboration. 2016d, *A&A*, 594, A22
- Planck Collaboration. 2016e, *A&A*, 594, A24
- Planck Collaboration. 2016f, *A&A*, 594, A26
- Planck Collaboration. 2016g, *A&A*, 596, A107
- Planck Collaboration. 2016h, *A&A*, 596, A108
- Rykoff, E. S. et al. 2016, *Astrophys. J. Suppl.*, 224, 1
- Sereno, M., Covone, G., Izzo, L., et al. 2017 [[arXiv:1703.06886](#)]
- Simet, M., Battaglia, N., Mandelbaum, R., & Seljak, U. 2015, in *American Astronomical Society Meeting Abstracts*, Vol. 225, American Astronomical Society Meeting Abstracts, 443.04
- Smith, G. P., Mazzotta, P., Okabe, N., et al. 2016, *MNRAS*, 456, L74
- Sunyaev, R. A. & Zeldovich, Ya. B. 1970, *Astrophys. Space Sci.*, 7, 20
- Tinker, J., Kravtsov, A. V., Klypin, A., et al. 2008, *ApJ*, 688, 709
- van Uitert, E., Joachimi, B., Joudaki, S., et al. 2017, *ArXiv e-prints* [[arXiv:1706.05004](#)]
- Vikhlinin, A., Kravtsov, A. V., Burenin, R. A., et al. 2009, *ApJ*, 692, 1060
- von der Linden, A., Mantz, A., Allen, S. W., et al. 2014, *MNRAS*, 443, 1973